



HAL
open science

Rotational relaxation of H₂S by collision with He

Otoniel Denis-Alpizar, Thierry Stoecklin

► **To cite this version:**

Otoniel Denis-Alpizar, Thierry Stoecklin. Rotational relaxation of H₂S by collision with He. *Astronomy and Astrophysics - A&A*, 2020, 638, 10.1051/0004-6361/202037821 . hal-03044204

HAL Id: hal-03044204

<https://cnrs.hal.science/hal-03044204>

Submitted on 7 Dec 2020

HAL is a multi-disciplinary open access archive for the deposit and dissemination of scientific research documents, whether they are published or not. The documents may come from teaching and research institutions in France or abroad, or from public or private research centers.

L'archive ouverte pluridisciplinaire **HAL**, est destinée au dépôt et à la diffusion de documents scientifiques de niveau recherche, publiés ou non, émanant des établissements d'enseignement et de recherche français ou étrangers, des laboratoires publics ou privés.

Rotational relaxation of H₂S by collision with He

Otoniel Denis-Alpizar¹ and Thierry Stoecklin²

¹ Núcleo de Astroquímica y Astrofísica, Instituto de Ciencias Químicas Aplicadas, Facultad de Ingeniería, Universidad Autónoma de Chile, Av. Pedro de Valdivia 425, Providencia, Santiago, Chile
e-mail: otoniel.denis@uautonoma.cl

² Institut des Sciences Moléculaires, Université de Bordeaux, CNRS UMR 5255, 33405 Talence Cedex, France
e-mail: thierry.stoecklin@u-bordeaux.fr

Received 25 February 2020 / Accepted 17 April 2020

ABSTRACT

Context. The H₂S molecule has been detected in several regions of the interstellar medium (ISM). The use of non-LTE models requires knowledge of accurate collisional rate coefficients of the molecules detected with the most common collider in the ISM.

Aims. The main goal of this work is to study the collision of H₂S with He.

Methods. A grid of ab initio energies was computed at the coupled cluster level of theory including single, double, and perturbative triple excitations (CCSD(T)) and using the augmented correlation consistent polarized quadruple zeta (aug-cc-pVQZ) basis set supplemented by a set of mid-bond functions. These energies were fitted to an analytical function, which was employed to study the dynamics of the system. Close coupling calculations were performed to study the collision of H₂S with He.

Results. The rate coefficients determined from the close coupling calculation were compared with those of the collision with H₂O+He, and large differences were found. Finally, the rate coefficients for the lower rotational de-excitation of H₂S by collision with He are reported.

Key words. astrochemistry – molecular data – molecular processes – scattering – ISM: molecules

1. Introduction

Sulfur molecules play an important role in biological systems on Earth, which increases the interest in following the chemical history of these molecules in the Universe (Fuente et al. 2017). Approximately 20 molecules containing sulfur have been detected in the interstellar medium (ISM), as can be seen in the Cologne Database for Molecular Spectroscopy (CDMS; Müller et al. 2005). Owing to their properties and abundance, these systems are useful tracers of interstellar material (Duley et al. 1980; Nagy et al. 2013; Fuente et al. 2016; Goicoechea et al. 2017; Gorai 2018; Cernicharo et al. 2018; Drozdovskaya et al. 2018).

Among all sulfur-bearing molecules, we focus on hydrogen sulfide (H₂S). This system has been observed in a variety of astrophysical environments (Thaddeus et al. 1972; Ukita & Morris 1983; Minh et al. 1989, 1990; Martin et al. 2005; Li et al. 2015; Holdship et al. 2016; Minh 2016; Phuong et al. 2018). H₂S has been used as a probe of sulfur chemistry in the ISM and also as a probe of the physical state of the gas (Crockett et al. 2014).

The local thermal equilibrium (LTE) can be employed to determine the physicochemical conditions of the region where the molecules are observed, for example, density, excitation temperature, and molecular abundance. In such a model, the rotational population of the molecule follows a Boltzmann distribution. However, in typical molecular clouds the density is low and collisions are rare. Also, the LTE does not apply, and non-LTE models should be considered. Such models require the input of both the Einstein coefficients, which are usually known, and accurate state-to-state collisional rate coefficients with the most common colliders of the ISM (e.g., He, H₂, H, and e⁻).

Recently, Crockett et al. (2014) studied the H₂S molecule in the Orion KL nebula and performed non-LTE analysis. In the absence of collisional rates for this system, these authors used two approximations. First, they employed the experimental depopulation cross section of Ball et al. (1999) for the 1_{1,0} → 1_{0,1} transition of H₂S+He to derive a base rate coefficient of 1.35 × 10⁻¹¹ cm³ s⁻¹ at 10 K. The collision rates were then scaled in proportion to radiative line strengths so that the sum of all downward rates from each upper state is equal to the base rate (Crockett et al. 2014). Second, Crockett et al. (2014) used the rates for the collisions of H₂O with H₂ to scale those for the collisions with H₂S. To conclude, it is important to point out that the rate coefficients available for H₂S in the LAMDA database (Schöier et al. 2005) are also those scaled from the collision with H₂O, while the spectroscopic characteristics of the H₂O and H₂S molecules are very different, and differences in the interaction potential energy surfaces (PESs) of He with H₂S and H₂O are most probable. A full set of collisional rates for H₂S is then required for evaluating the validity of these two approximations.

A very recent work dedicated to the collisions of H₂ with H₂S (Dagdigian 2020) was published online at the same time as the present work was submitted to publication. A brief comparison of the rates for collision of H₂S with He and H₂ are therefore used to discuss the validity of the mass scaling procedure for estimating the rates for collisions with H₂ from those with He.

The main goal of this paper is to provide a new set of reliable rotational rate coefficients for the collision of H₂S with He calculated at the close coupling level on a new ab initio PES. This article is organized as follows: In the next section, the methods used are presented. In Sect. 3, the results are discussed, while the conclusions can be found in Sect. 4.

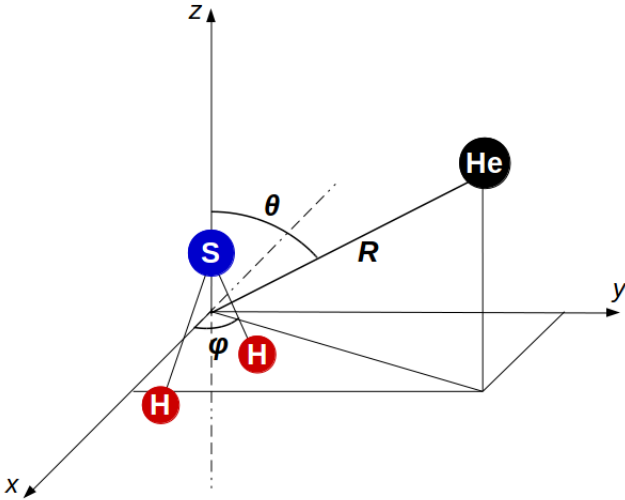


Fig. 1. Internal coordinates used to describe the H₂S+He system.

2. Methods

2.1. Ab initio calculations

A large grid of interaction ab initio energies were computed to study the H₂S+He complex. The calculations were performed at the coupled cluster level of theory including single, double, and perturbative triple excitations (CCSD(T); Raghavachari et al. 1989) and using the augmented correlation consistent polarized quadruple zeta (aug-cc-pVQZ; Dunning 1989) basis set supplemented by a set of mid-bond functions (Cybulski & Toczyłowski 1999). The basis set superposition error was corrected using the counterpoise procedure (Boys & Bernardi 1970). The calculations were performed with the MOLPRO package (Werner et al. 2012). The center of the coordinates of the system was located at the center of mass of H₂S molecule, H₂S is in the plane *xz*, and the scattering coordinates *R*, *θ*, and *φ* are defined in Fig. 1.

The rigid rotor approximation is used to describe the H₂S molecule and the HS bond length $r_{S-H} = 1.35 \text{ \AA}$ and bond angle $\langle \text{HS} \rangle = 92.13^\circ$ are fixed to their vibrationally averaged value in the rovibrational ground state Cook et al. (1975). The radial grid includes 25 values of *R* ranging from 1.5 Å to 9 Å, while *θ* and *φ* vary from 0° to 180° in steps of 10° and 15°, respectively. A total of 6175 ab initio energies were computed.

2.2. Analytical representation of the PES

The ab initio energies were fitted to the following analytical form:

$$V(R, \theta_1, \theta_2, \phi) = \sum_{l=0}^8 \sum_{m=0}^{\min(l,6)} f_{l,m}(R) \bar{P}_l^m(\cos \theta) \cos(m\phi), \quad (1)$$

where the angular part is represented by a product of normalized associated Legendre and cosine functions, and *m* is even. For each *R* value, the ab initio energies were fitted to this analytical form using a least-squares procedure. Then, the $f_{l,m}$ radial coefficients were obtained using a reproducing kernel Hilbert space (RKHS) representation,

$$f_{l,m}(R) = \sum_{k=1}^N \alpha_k^{l,m} q^{5,2}(R, R_k) \quad (2)$$

with

$$q^{5,2}(R, R_k) = \frac{2}{21R_{>}^6} - \frac{R_{<}}{14R_{>}^7}, \quad (3)$$

where *N* is the number of radial points of the grid and $q^{5,2}(R, R_k)$ are the one-dimensional kernels defined by Ho and Rabitz (Ho & Rabitz 1996). The $\alpha_k^{l,m}$ coefficients are found by solving the linear system $\mathbf{f}_{lm}(R_i) = \alpha^{l,m} \mathbf{q}(R_i, R_j)$, where *i* and *j* label different radial grid points, while the use of the $q^{5,2}(R, R_k)$ kernel ensures a R^{-6} long-range behavior (Soldán & Hutson 2000).

2.3. Dynamics

The dynamics of the system was studied by separately solving the close coupling equation for the two nuclear spin modifications of H₂S in the space-fixed frame. The calculations were performed with the most recent version of the Newmat code Stoecklin et al. (2019) and the log-derivative propagator.

The rotational constants of H₂S were fixed to their experimental values $A_0 = 10.3601 \text{ cm}^{-1}$, $B_0 = 9.0156 \text{ cm}^{-1}$, and $C_0 = 4.7318 \text{ cm}^{-1}$ (Cook et al. 1975), while the rotational basis set was made of 10 values of the rotational quantum number *j*. This included 50 ortho rotational states up to 908.085 cm⁻¹ and 50 para states up to 908.065 cm⁻¹. In what follows, we use the notation j_{K_A, K_C} to designate the asymmetric top rotational energies of H₂S, where K_A and K_C are, respectively, the absolute values of the *Z* molecular axis projections of the rotational angular momentum *j* in the limit of a prolate or an oblate top. This molecule is a near-oblate asymmetric top, and the oblate-limit projection quantum number K_C is then an approximately good quantum number. This is in contrast with water, which is an intermediate case closer to a prolate limit for which neither K_A nor K_C are nearly conserved. Scattering calculations were carried out for energies up to 4000 cm⁻¹ for each H₂S–He pair of nuclear spin modifications. This range of energies could involve excited bending and stretching levels of H₂S, while the H₂S vibration is not taken into account in the present work. We know however from previous work (Stoecklin et al. 2019) that the state-to-state rotational excitation uncertainty resulting from the use of this approximation above the excited vibrational level thresholds of H₂S is very small as rovibrational cross sections are two orders of magnitude smaller than purely rotational cross section. Partial waves up to total angular momentum $J = 90$ were included in the calculations to achieve a 10⁻³ relative criterion for the convergence of the state-selected quenching cross section as a function of the maximal value of the total angular momentum quantum number *J*. The maximum propagation distance was 50 bohr, and convergence was checked as a function of the propagator step size. The computed state-to-state integral cross sections $\sigma_{j_{K_A, K_C} \rightarrow j'_{K'_A, K'_C}}$ were eventually employed to calculate the corresponding state-selected rate coefficients $k_{j_{K_A, K_C} \rightarrow j'_{K'_A, K'_C}}(T)$ between 1 and 1000 K by Boltzmann averaging over the collision energy E_c , that is,

$$k_{j_{K_A, K_C} \rightarrow j'_{K'_A, K'_C}}(T) = \sqrt{\frac{8}{\pi\mu}} (k_B T)^{-\frac{3}{2}} \int_0^\infty \sigma_{j_{K_A, K_C} \rightarrow j'_{K'_A, K'_C}} e^{-\frac{E_c}{k_B T}} E_c dE_c. \quad (4)$$

3. Results

3.1. PES

The grid of ab initio energies was fitted to the analytical form of Eq. (1). The two panels of Fig. 2 shows contour plots of the resulting PES for $\phi = 0^\circ$ and $\phi = 90^\circ$, respectively. The

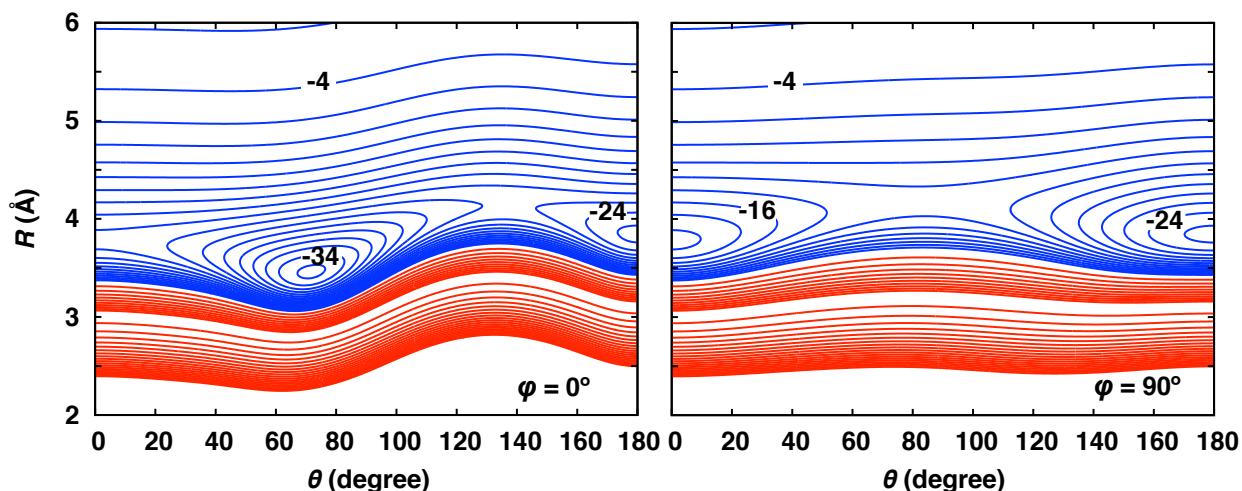


Fig. 2. Contour plots of the H₂S+He system at $\varphi = 0^\circ$ (panel A) and $\varphi = 90^\circ$ (panel B). Red contour lines correspond to positive energies ranging from 0 to 100 cm⁻¹ in steps of 10 cm⁻¹, and in steps of 100 cm⁻¹ in the [100, 2000] cm⁻¹ interval. Blue contour lines show the negative energies varying in steps of 2 cm⁻¹.

global minimum of the PES (-36.49 cm⁻¹) appearing on the left panel of this figure is associated with the bent configuration ($R = 3.46$ Å, $\theta = 72^\circ$, $\varphi = 0^\circ$). A secondary minimum, at $R = 3.84$ Å and $\theta = 180^\circ$ (φ is undefined for $\theta = 0^\circ$ and 180°), can be seen on this figure. The global minimum energy of H₂S+He PES is then very close to that of the H₂O+He system (-34.9 cm⁻¹) (Patkowski et al. 2002), which is also associated with a similar geometry of the complex ($R = 3.13$ Å, $\theta = 75^\circ$, $\varphi = 0^\circ$). As a result, the magnitudes of the cross sections should approximately follow the scaling law based on the ratio of the reduced masses of the two systems used in the Lambda database (Schöier et al. 2005). Conversely, the angular anisotropies of the two PES are very different because the H₂O+He PES does not exhibit any secondary minimum, as shown in Fig. 3 of Patkowski et al. (2002). As a result and because of the consequences of the differences between the values of the rotational constants of H₂O and H₂S discussed in Sect. 2.3, the propensity rules followed by the rotational transitions of the two collisional systems are expected to differ.

3.2. Dynamics

Figures 3 and 4 show de-excitation cross sections from examples of para ($K_a + K_c$ even) and ortho ($K_a + K_c$ odd) states of the $j = 2$ and $j = 4$ multiplets. In each figure, the lower and upper panels are dedicated to examples of initial para and ortho states, respectively. These are on one side the ($j = 2$, $K_a = 2$, $K_c = 0$) and ($j = 4$, $K_a = 4$, $K_c = 0$) para states and on the other the ($j = 2$, $K_a = 2$, $K_c = 1$) and ($j = 4$, $K_a = 4$, $K_c = 1$) ortho state of H₂S. Before analyzing these figures we note that all these transitions tend to follow the general propensity rule demonstrated by Alexander (1982). This early paper states that transitions between states with the same sign of the parity index $\epsilon = (-)^{j+K_a+K_c}$ are favored, and the collisional selectivity becomes increasingly rigorous as both j and the collisional energy increase. In order to simplify the notation, in the following we only give the three integers mnp to designate the $j = m$, $K_a = n$, $K_c = p$ level.

If we first look at the transitions issued from the 2 2 1 ortho level of H₂S represented in the upper panel of Fig. 3, we see that the 2 1 2 final level gives the largest cross section in the [1–100] cm⁻¹ interval. This is expected as this transition is

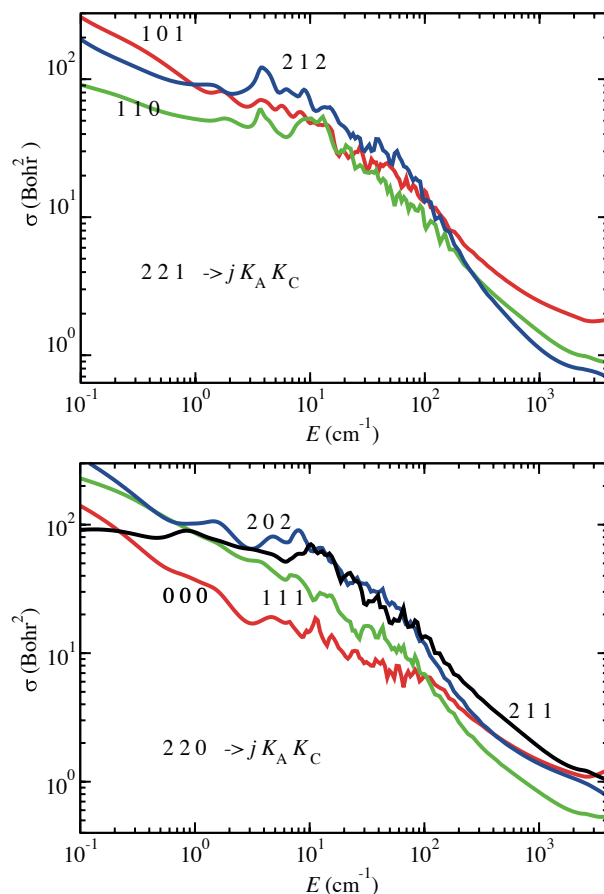


Fig. 3. Rotational de-excitation cross sections of H₂S by collision with He. The upper and lower panels show transitions issued from the 2 2 1 and 2 2 0 initial levels of H₂S, respectively.

elastic in j ($\Delta j = 0$), while these two levels have the same parity index and are the closest in energy. They however differ in K_c ($\Delta K_c = 1$), whereas H₂S is a near-oblate symmetric top and K_c should then nearly be a good quantum number. At higher collisional energy, the ($\Delta K_c = 0$) propensity rule is conversely respected as the 1 0 1 final level gives the largest cross section.

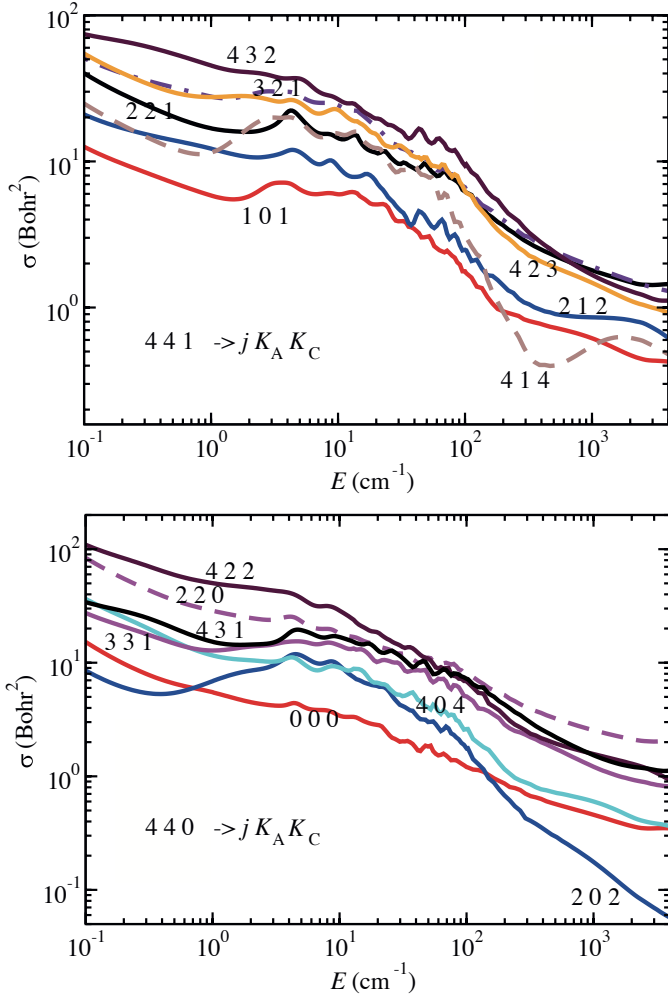


Fig. 4. Rotational de-excitation cross sections of H₂S by collision with He. The upper and lower panels show transitions issued from the 4 4 1 and 4 4 0 initial levels of H₂S, respectively.

Similar behavior can be observed for the transitions issued from the initial 2 2 0 para state represented in the lower panel of the same Fig. 3). The 2 1 1 level followed by the 2 0 2 level are closest in energy, have the same parity index as 2 2 0, and are j elastic. Again these two transitions give the largest cross section in the [1–100] cm⁻¹ interval. At higher energy ($\Delta K_c = 0$) propensity rule makes the 0 0 0 transition progressively increase, whereas it is inelastic in j ($\Delta j = 2$) and is the most distant in energy.

If we now look at the transitions issued from the 4 4 1 ortho level represented in the upper panel of Fig. 4, we see that again the 4 3 2 and 4 2 3 levels, which are the closest in energy with the same parity index, give the highest cross section up to 300 cm⁻¹. However, the 3 2 1 level, whose parity index is opposite, is inelastic in j ($\Delta j = 1$) and is quite distant in energy. But this level follows the ($\Delta K_c = 0$) propensity rule giving cross sections that are very close in magnitude and become largest at higher energy. Similar behavior can be observed in the lower panel of Fig. 4 for the transitions issued from the 4 4 0 para level. The 2 2 0 level, which is quite distant in energy and is inelastic in j ($\Delta j = 2$), gives the largest cross section above 100 cm⁻¹. We conclude that the ($\Delta K_c = 0$) propensity rule becomes increasingly rigorous as j and the collision energy both increase, while for collision energy below the well depth, it is rather the conservation of the parity

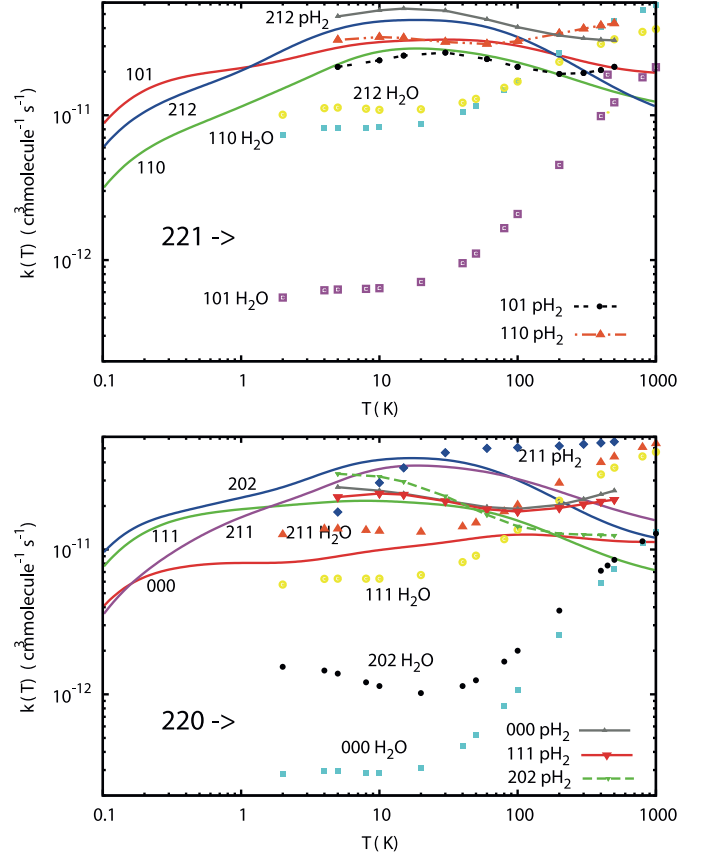


Fig. 5. Rotational de-excitation rate coefficients of H₂S by collision with He. The upper and lower panels show transitions issued from the 2 2 1 and 2 2 0 initial levels of water, respectively. The rates are compared with the corresponding rates for the H₂S + para-H₂ collisions (designated by pH₂) and with those for H₂O+He collisions (designated by H₂O).

index and the lowest energy difference that lead to the highest transition cross sections.

We now turn to the comparison between the H₂S+He and H₂O+He collisional systems as we have seen that the well depths of the two associated PES are very close, while the ratio of the reduced masses of the two systems nearly equals one. These are two reasons that lead several authors to assume that the collisional rate coefficients would also be equal. The rotational de-excitation rate coefficients of H₂S by collision with He from the initial states 2 2 1 and 2 2 0 of H₂S are shown in the upper and lower panels of Fig. 5, respectively, where they are compared with those reported for the H₂O+He system by Yang et al. (2013), which can be found in the Basecol database (Dubernet et al. 2013). All three temperature dependence, magnitude, and propensity rules differ strongly for the two systems. These strong differences result from both the differences in the angular anisotropies of the two PESs and the rotational constants; H₂S has a nearly oblate symmetric top, while H₂O is a good example of an asymmetric top intermediate case. The data in this work computed will be sent to the Basecol database soon.

We then compare our results with the only experimental data available of Ball et al. (1999) for the 1₁₀ → 1₀₁ transition of H₂S colliding with He. As a matter of fact, PES calculations have reached a very high level of accuracy, which is illustrated by the very good agreement between theory and experiment obtained in several recent studies dedicated to the

H₂-CO (Faure et al. 2016), D₂-CO (Stoecklin et al. 2017), Ar-CO (Mertens et al. 2017), NO+O₂ (Gao et al. 2018), and ND₃-D₂ (Gao et al. 2019) systems. Ball et al. (1999) did not obtain state-to-state rate coefficients but gave instead depopulation Boltzmann averaged cross sections for the rotational transition $1_{01} \rightarrow 1_{10}$ as a function of temperature. They neglected the contribution of higher notational levels of H₂S and used an approximate two-level model, which is expected to be valid up to approximately 10 K. They reported a value of 6.84 \AA^2 for the depopulation cross section of the 110 level of H₂S at 11.1 K or equivalently a value of $1.75 \cdot 10^{-11} \text{ cm}^3 \text{ molecule}^{-1} \text{ s}^{-1}$ for the corresponding rate at this temperature. Our calculated value is about three times larger ($5.7 \cdot 10^{-11} \text{ cm}^3 \text{ molecule}^{-1} \text{ s}^{-1}$). Such an agreement between theory and experiment, if not satisfactory, is understandable knowing that energy resonances in this domain of energy may drastically change the magnitude of the cross sections in a very narrow energy interval, while possible sources of experimental error are mentioned by these authors. In the same publication Ball et al. (1999) also performed close coupling calculations and obtained a good agreement with experiment at this temperature. This agreement however appears to be fortuitous as they used an approximate model of PES whose well depth is only a half of ours. Other experimental data are then needed to decide if there is a real disagreement between theory and experiment.

To conclude, we also compared in the upper and lower panels of Fig. 5 the rotational de-excitation rate coefficients of H₂S by collision with He from the initial states $2\ 2\ 1$ and $2\ 2\ 0$ of H₂S with those recently published by Dagdigian (Dagdigian 2020) for the collisions with H₂. The well depth of the H₂-H₂S complex (146.8 cm^{-1}) calculated by Dagdigian (2020) is five times deeper than that of He-H₂S, while the relative masses of the former is about a half of the later. In Fig. 5, the rate coefficients for the two systems are seen to be about of the same magnitude, while differing both in the law variation as a function of temperature and in the propensity rules. The scaling law based on the square root of the inverse ratio of the relative masses therefore does not appear to be a good option to predict the rate coefficients for the collisions of H₂S with para-H₂ from those with He, while the excitation rate coefficients with He need to be included in the modeling of the rotational excitation of H₂S.

4. Summary

A three-dimensional PES for the collision of H₂S+He was developed. The global minimum (-36.49 cm^{-1}) is obtained for a bent geometry and is comparable in both aspects to that of the He-H₂O system, while a secondary minimum is identified that does not exist for He-H₂O. Close coupling calculations were performed for the 50 lowest rotational states of the two nuclear spin modifications of H₂S. At low and intermediate energy, the transition toward levels that are the closest in energy and have the same parity index gives the largest cross section, while for higher energies the near-oblate ($\Delta K_C = 0$) propensity rule progressively takes the lead. Our calculation gives a value that is the triple of the only experimental data available for the $1_{01} \rightarrow 1_{10}$ depopulation rate coefficient at 10 K. However, this comparison is not conclusive and more experimental data will be needed.

While the existing databases suggested up to now to use the He-H₂O state-to-state rate coefficients for the He-H₂S collisions, we demonstrated that the three temperature dependence, magnitude and propensity rules differ strongly for the two systems. These strong differences result from both the differences in the angular anisotropies of the two PESs and in the rotational constants, where H₂S has a nearly oblate symmetric top while H₂O

is a good example of asymmetric top intermediate case. We also compared our results with those by Dagdigian (2020) for the collisions with H₂. The rate coefficients for the two systems were found to be about of the same magnitude, but these rates differ in the law variation as a function of temperature and in the propensity rules. We then recommend using both the new state-to-state rate coefficients with He and H₂ in any non-LTE analysis of astronomical observation of H₂S.

Acknowledgements. We acknowledge the support from the ECOS-SUD-CONICYT project number C17E06 (Programa de Cooperación Científica ECOS-CONICYT ECOS170039). We also thank Paul Dagdigian for the valuable discussion and for providing the data for the collision H₂S+H₂. Computer time for this study was provided by the Mésocentre de Calcul Intensif Aquitain, which is the computing facility of Université de Bordeaux et Université de Pau et des Pays de l'Adour.

References

- Alexander, M. H. 1982, *J. Chem. Phys.*, **77**, 1855
 Ball, C. D., Mengel, M., De Lucia, F. C., & Woon, D. E. 1999, *J. Chem. Phys.*, **111**, 8893
 Boys, S. F., & Bernardi, F. 1970, *Mol. Phys.*, **19**, 553
 Cernicharo, J., Lefloch, B., Agúndez, M., et al. 2018, *ApJ*, **853**, L22
 Cook, R. L., De Lucia, F. C., & Helminger, P. 1975, *J. Mol. Struct.*, **28**, 237
 Crockett, N., Bergin, E., Neill, J., et al. 2014, *ApJ*, **781**, 114
 Cybulski, S. M., & Toczyłowski, R. 1999, *J. Chem. Phys.*, **111**, 10520
 Dagdigian, P. J. 2020, *J. Chem. Phys.*, **152**, 074307
 Drozdovskaya, M. N., van Dishoeck, E. F., Jørgensen, J. K., et al. 2018, *MNRAS*, **476**, 4949
 Dubernet, M., Alexander, M., Ba, Y., et al. 2013, *A&A*, **553**, A50
 Duley, W., Millar, T., & Williams, D. 1980, *MNRAS*, **192**, 945
 Dunning, T. H. 1989, *J. Chem. Phys.*, **90**, 1007
 Faure, A., Jankowski, P., Stoecklin, T., & Szalewicz, K. 2016, *Sci. Rep.*, **6**, 28449
 Fuente, A., Cernicharo, J., Roueff, E., et al. 2016, *A&A*, **593**, A94
 Fuente, A., Goicoechea, J. R., Pety, J., et al. 2017, *ApJ*, **851**, L49
 Gao, Z., Karman, T., Tang, G., et al. 2018, *Phys. Chem. Chem. Phys.*, **20**, 12444
 Gao, Z., Loreau, J., van der Avoird, A., & van de Meerakker, S. Y. 2019, *Phys. Chem. Chem. Phys.*, **21**, 14033
 Goicoechea, J. R., Cuadrado, S., Pety, J., et al. 2017, *A&A*, **601**, L9
 Gorai, P. 2018, *Exploring the Universe: From Near Space to Extra-Galactic* (Springer), p467–475
 Ho, T. S., & Rabitz, H. 1996, *J. Phys. Chem.*, **104**, 2584
 Holdship, J., Viti, S., Jimenez-Serra, I., et al. 2016, *MNRAS*, **463**, 802
 Li, J., Wang, J., Zhu, Q., Zhang, J., & Li, D. 2015, *ApJ*, **802**, 40
 Martin, S., Martin-Pintado, J., Mauersberger, R., Henkel, C., & García-Burillo, S. 2005, *ApJ*, **620**, 210
 Mertens, L. A., Labiad, H., Denis-Alpizar, O., et al. 2017, *Chem. Phys. Lett.*, **683**, 521
 Ahmed Zewail (1946–2016) Commemoration Issue of Chemical Physics Letters
 Minh, Y. 2016, *J. Phys. Conf. Ser.*, **728**, 052007
 Minh, Y., Irvine, W. M., & Ziurys, L. M. 1989, *ApJ*, **345**, L63
 Minh, Y., Ziurys, L. M., Irvine, W. M., & McGonagle, D. 1990, *ApJ*, **360**, 136
 Müller, H. S., Schlöder, F., Stutzki, J., & Winnewisser, G. 2005, *J. Mol. Struct.*, **742**, 215
 Nagy, Z., Van der Tak, F., Ossenkopf, V., et al. 2013, *A&A*, **550**, A96
 Patkowski, K., Korona, T., Moszynski, R., Jeziorski, B., & Szalewicz, K. 2002, *J. Mol. Struct. (Theochem.)*, **591**, 231
 Phuong, N., Chapillon, E., Majumdar, L., et al. 2018, *A&A*, **616**, L5
 Raghavachari, K., Trucks, G. W., Pople, J. A., & Head-Gordon, M. 1989, *Chem. Phys. Lett.*, **157**, 479
 Schöier, F. L., van der Tak, F. F. S., van Dishoeck, E. F., & Black, J. H. 2005, *A&A*, **432**, 369
 Soldán, P., & Hutson, J. M. 2000, *J. Chem. Phys.*, **112**, 4415
 Stoecklin, T., Faure, A., Jankowski, P., et al. 2017, *Phys. Chem. Chem. Phys.*, **19**, 189
 Stoecklin, T., Denis-Alpizar, O., Clergerie, A., et al. 2019, *J. Phys. Chem. A*, **123**, 5704
 Thaddeus, P., Kutner, M., Penzias, A., Wilson, R., & Jefferts, K. 1972, *ApJ*, **176**, L73
 Ukita, N., & Morris, M. 1983, *A&A*, **121**, 15
 Werner, H.-J., Knowles, P. J., Knizia, G., Manby, F. R., & Schütz, M. 2012, *WIREs Comput. Mol. Sci.*, **2**, 242
 Yang, B., Nagao, M., Satomi, W., Kimura, M., & Stancil, P. 2013, *ApJ*, **765**, 77